Science Advances
AAAS

advances.sciencemag.org/cgi/content/full/6/38/eabc6414/DC1

Supplementary Materials for

Reprogrammable shape morphing of magnetic soft machines

Yunus Alapan, Alp C. Karacakol, Seyda N. Guzelhan, Irem Isik, Metin Sitti*

*Corresponding author. Email: sitti@is.mpg.de

Published 18 September 2020, *Sci. Adv.* **6**, eabc6414 (2020)
DOI: 10.1126/sciadv.abc6414

The PDF file includes:

Other Supplementary Material for this manuscript includes the following:

(available at advances.sciencemag.org/cgi/content/full/6/38/eabc6414/DC1)

Computational modeling of the magnetic soft elastomers. Design of the magnetic soft structures takes both the geometry and the magnetization profile into consideration for controlled shape changing. Intuitive designs can be used for simple shape changes under external magnetic fields, but more demanding and complex deformations require a predictive model. We have developed a predictive model utilizing COMSOL and a custom MATLAB script to solve for the quasi static state of the magnetic soft structures.

Magnetic soft structures are subjected to magnetic forces ($\boldsymbol{f}$), magnetic torques ($\boldsymbol{\tau}$), and gravitational forces ($m\boldsymbol{g}$), which creates stresses on the soft body which deforms to minimize the total magnetic and elastic potential energy. Moreover, direction of magnetic forces and torques changes along with the magnetization direction during deformation, creating a distributed heterogeneous response to the external magnetic fields over the structure. To capture this heterogeneous response, each sample geometry is divided into smaller subsections labeled by 'i' with the pre-defined dimensions of d_x, d_y, d_z and magnetic moment of $\boldsymbol{m}^i$ (fig. S7A, B). Magnetic forces and torques for each subsection are calculated in a custom MATLAB script according to the applied magnetic field ($\boldsymbol{B}$) and the magnetic moment of each sub-section. Calculated magnetic forces ($\boldsymbol{f}^i = \boldsymbol{\nabla}(\boldsymbol{m}^i \cdot \boldsymbol{B})$) then applied as directional forces to the sub-sections. On the other hand, magnetic torques ($\boldsymbol{\tau}^i = \boldsymbol{m}^i \times \boldsymbol{B}$) are distributed as forces on the facets of the subsections. To achieve this, magnetic torque ($\boldsymbol{\tau}^i$) is separated into its orthogonal components ($\tau_x^i, \tau_y^i, \tau_z^i$) for a chosen Cartesian reference frame (fig. S7C). Then, these torque components are converted to the facet forces $f_{\tau_x}^i, f_{\tau_y}^i, f_{\tau_z}^i$ (fig. S7D). The directions of the forces on the facets are determined by following the right-hand rule, while their magnitudes are calculated as follows:

$$\left|f_{\tau_x}^i\right| = \frac{\tau_x^i}{d_z\ /2}\ ,\ \left|f_{\tau_y}^i\right| = \frac{\tau_y^i}{d_x\ /2}\ ,\ \left|f_{\tau_z}^i\right| = \frac{\tau_z^i}{d_y\ /2}\ , \tag{1}$$

where $f_{\tau_x}^i, f_{\tau_y}^i, f_{\tau_z}^i$ are the torque-induced forces due to the torques $\tau_x^i, \tau_y^i, \tau_z^i$, respectively. These forces are then transferred to the COMSOL via LiveLink, and structural mechanics module is used to solve for the elastic deformation of the magnetic soft structures. After every iteration, magnetic forces and torques are recalculated according to the updated magnetization direction vector in each subsection at deformed state until an equilibrium was reached.

Validation of the model is performed by using a beam structure with dimension of 10 mm length x 1 mm width x 0.17 mm thickness. Beam is magnetized along its long axis and fixed at 1.25 mm from one end. Then, magnetic fields in the range of 0 to 56 mT applied vertical to the magnetization direction of the beam. Both experimental and simulation results are obtained for the same conditions (fig. S7E). Deflection angle θ is calculated for both experimental and simulation results and compared (fig. S7F). The developed computational approach captures the deformation characteristics and is in good agreement with the experimental results.

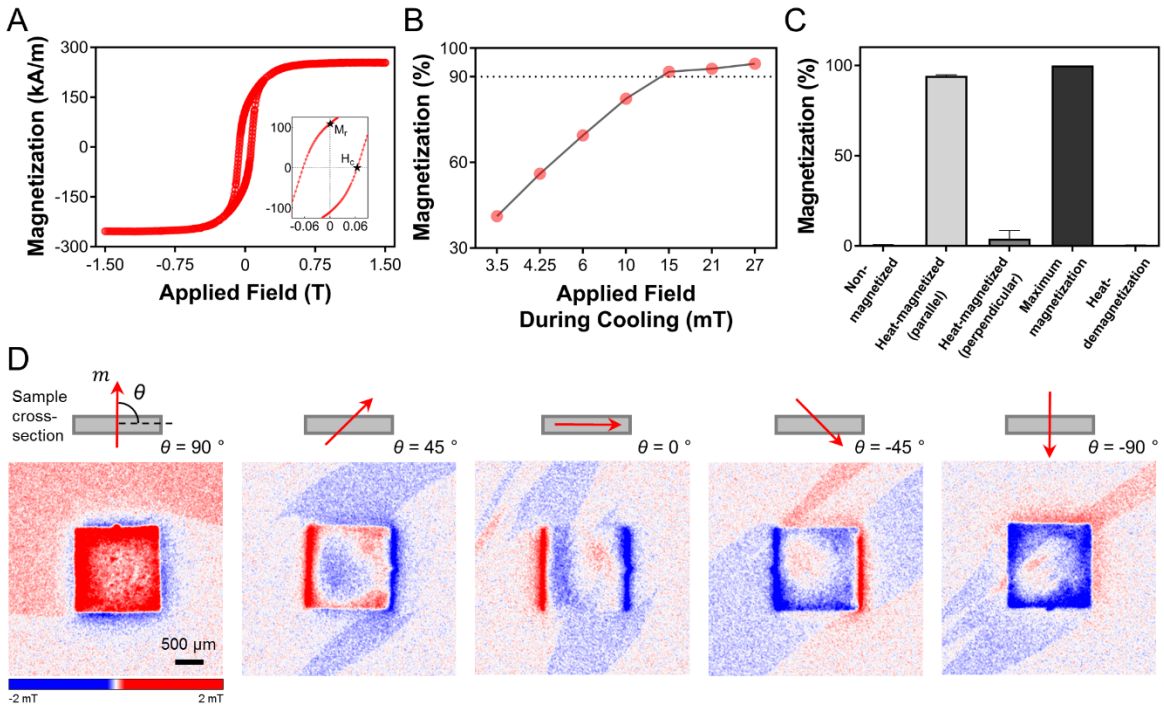

Figure S1. Magnetic properties, heat-assisted magnetization efficiency, and magnetic flux density measurements of the magnetic soft elastomer. (A) Hysteresis loop of the CrO_2 at room temperature. Remanent magnetization (M_r) of CrO_2 particles is 109 kA/m and their coercivity is 67 mT. **(B)** Effect of applied magnetic field strength during cooling on magnetization efficiency. **(C)** Heat-assisted magnetization efficiency in directions parallel and perpendicular to the magnetization direction and heat-assisted demagnetization. Magnetization values for samples magnetized under uniform 1.8 T field were considered as 100%. Error bars represent the standard deviation of the mean. **(D)** Measured out-of-plane magnetic flux density profiles of a rectangular magnetic soft elastomer sample magnetized in varying directions.

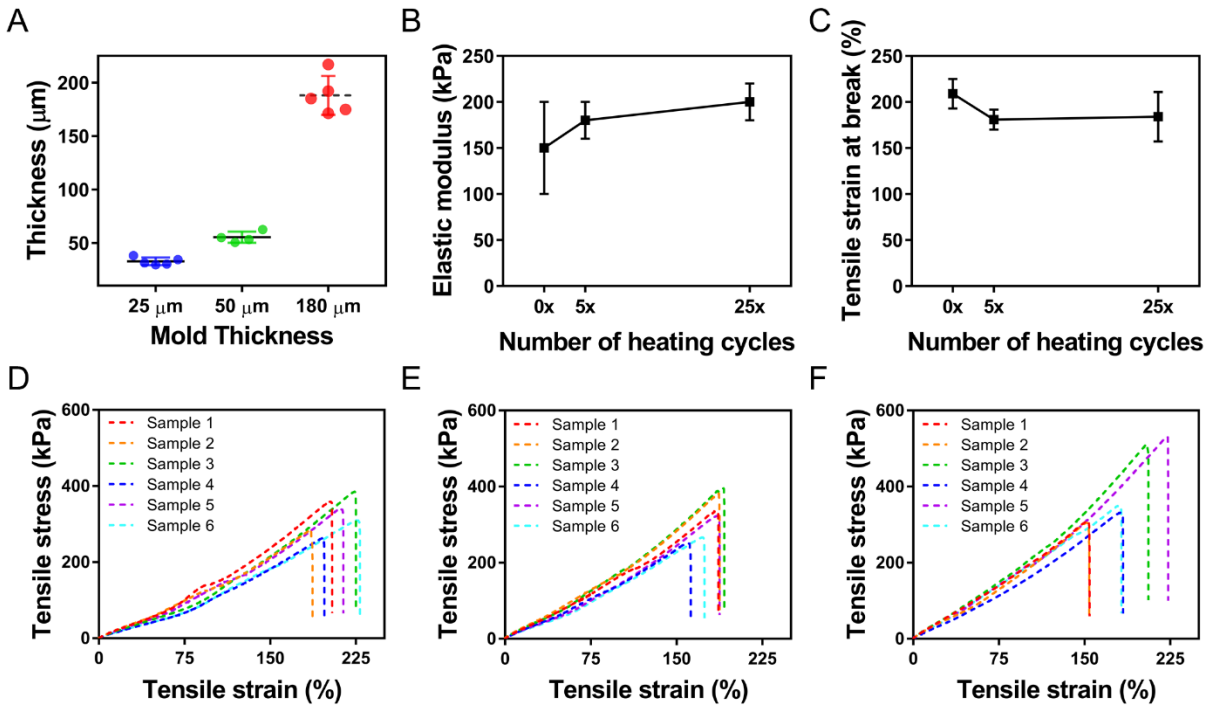

Figure S2. Mechanical properties of the magnetic soft elastomer. (A) Film thickness of the fabricated magnetic soft elastomers is controlled by changing the mold depth between 25 μm to 200 μm. **(B, C)** Elastic modulus (*E*) and tensile strain of the magnetic soft elastomers at break for heating cycles of 0, 5, and 25 above 150 °C. Error bars represent the standard deviation of the mean. **(D, E, F)** Stress-strain curves for the magnetic soft elastomers for heating cycles of 0, 5, and 25, respectively.

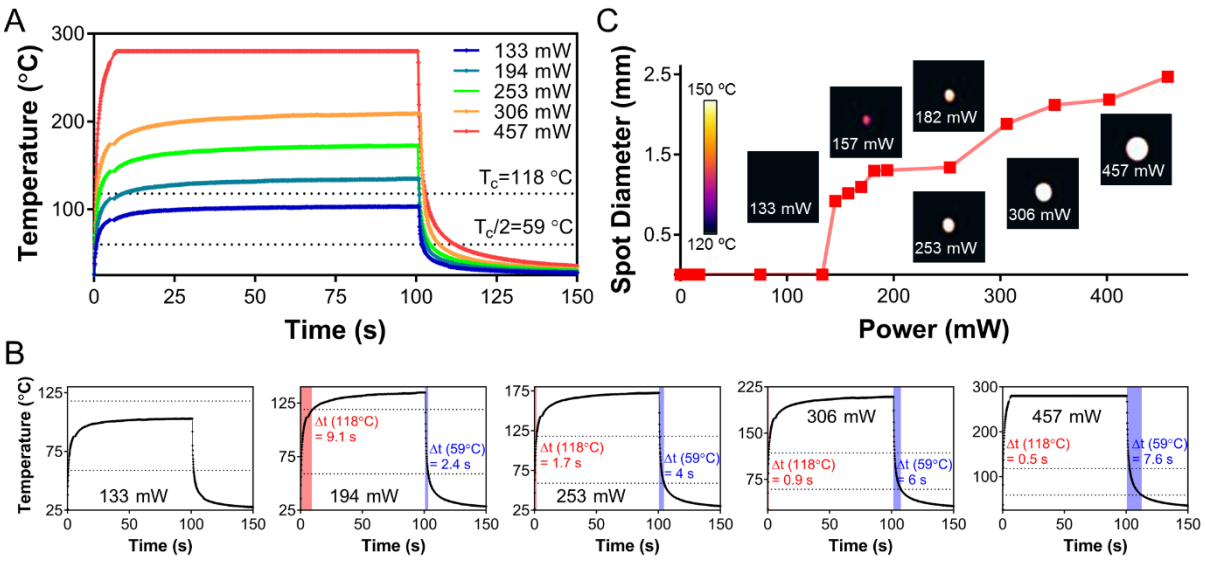

Figure S3. Photothermal response of the magnetic soft elastomer. (A, B) Effect of laser power on average temperature **(A)** and heating-cooling durations **(B)** of the magnetic soft elastomers. **(C)** Effect of laser power on spot diameter heated above the Curie temperature of CrO_2.

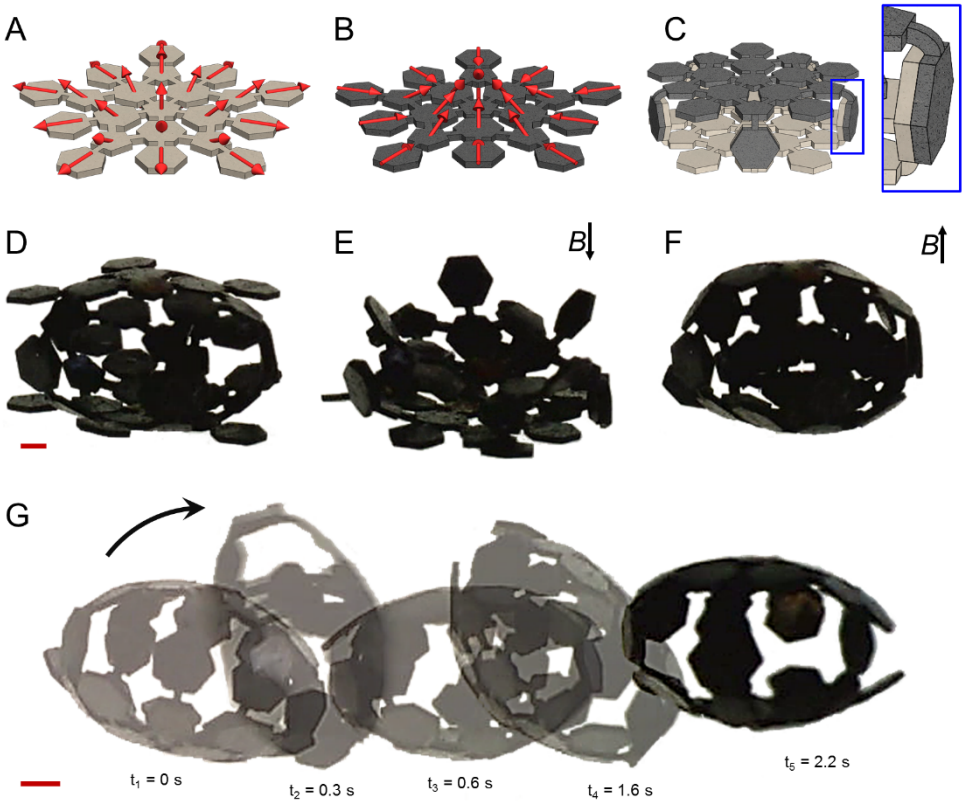

Figure S4. Stacked two half-sphere structures transform into a full sphere upon magnetic actuation. (A, B) Magnetization directions of the two half-sphere structures. **(C)** Manual assembly of the two-half ball structures realized by sticking together the corresponding hexagonal parts at the periphery, as shown in the inset. **(D-F)** Out-of-plane compression and formation of a closed spherical structure upon magnetic actuation (60 mT) in the directions indicated with the black arrows. **(G)** Rotational magnetic actuation results in rolling of the spherical structure while preserving its closed formation. Scale bars are 1 mm.

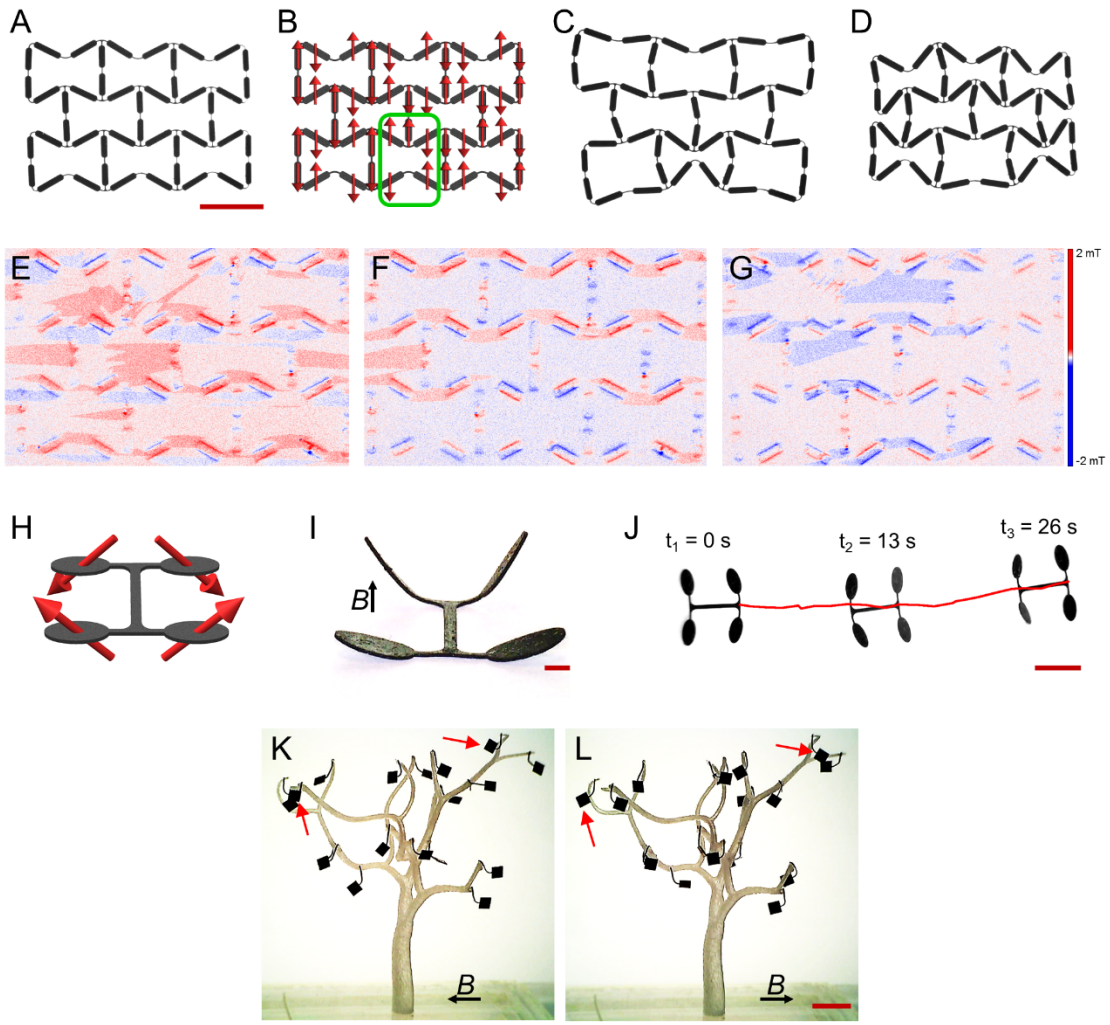

Figure S5. Reprogrammable magnetization of magnetic soft machines. (A-D) Reprogramming the magnetization profile of a single unit in the auxetic metamaterial results in heterogeneous deformation within the structure. Red arrows indicate local magnetization directions. Green solid lines show the reprogrammed regions. Scale bar is 5 mm. **(E-G)** Out-of-plane magnetic flux density profile measurements of the auxetic metamaterials shown in Fig. 3E **(E)**, Fig. S5B **(F)**, and Fig. 3H **(G).** Color bars indicate magnetic flux density strength. **(H-J)** Reprogramming magnetization profile of a quadrupedal flexible robot enables tunable locomotion pattern. **(H, I)** Upon magnetic actuation (20 mT) indicated with the black arrows, the legs deform in accordance with their magnetization directions. Scale bar is 1 mm. **(J)** The quadrupedal flexible robot locomote in a linear trajectory under rotational magnetic field actuation. Scale bar is 5 mm. **(K, L)** Reprogrammable magnetization of flexible magnetic leaves. Magnetization direction of two leaves (as shown with the red arrows) are reprogrammed in the opposite direction of the remaining leaves. Magnetic actuation (60 mT in the directions indicated with the black arrows) resulted in their reverse deformation compared to the other leaves. Scale bar is 5 mm.

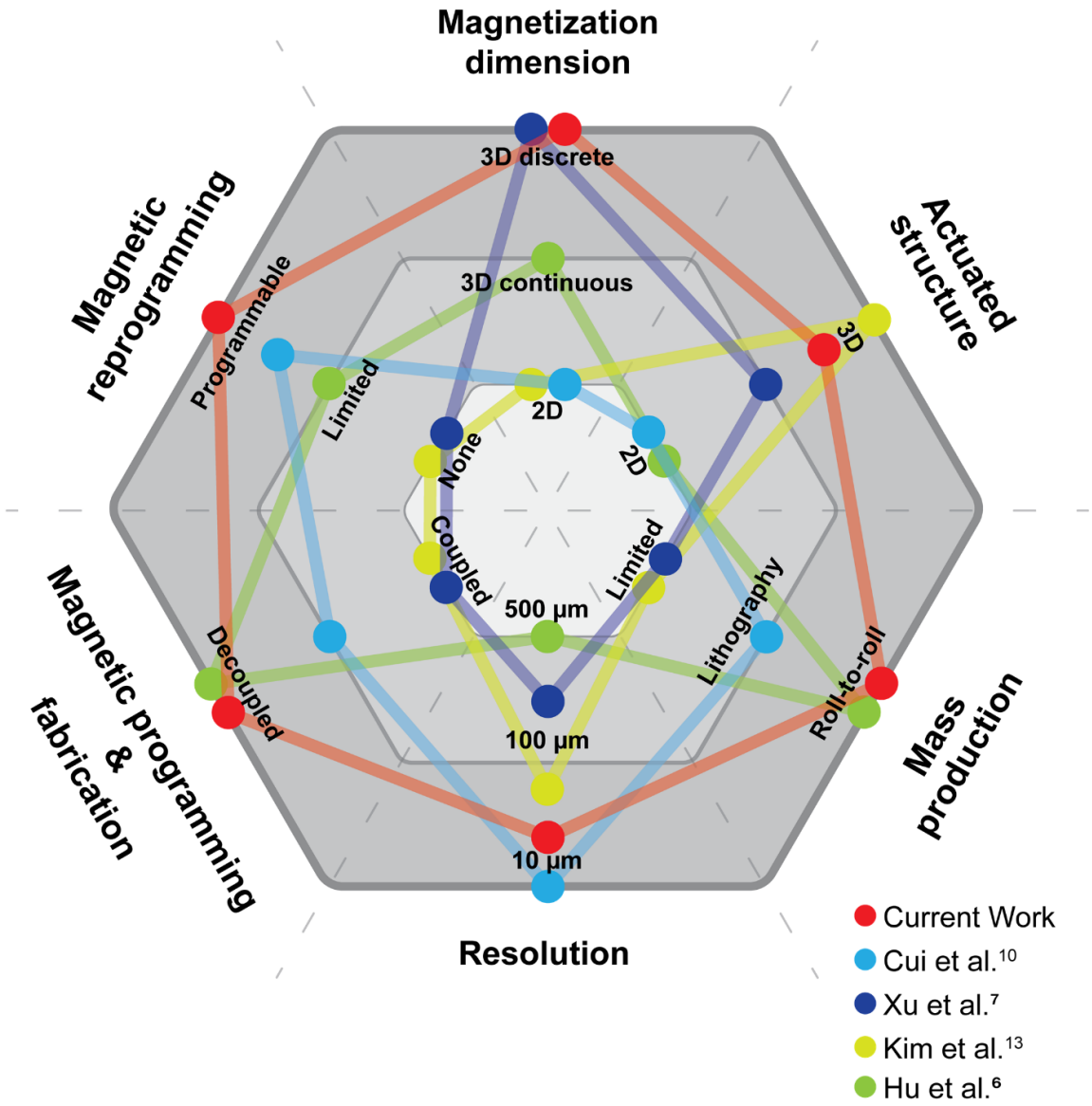

Figure S6. Performance comparison of previous magnetic soft material programming approaches with the current study. Magnetization and related fabrication capabilities of our heat-assisted magnetic programming strategy are compared with those of existing magnetic programming approaches for soft materials in the literature (*6, 7, 10, 13*). Magnetization dimension indicates the degree of freedom available for magnetization, where 3D refers to the capability to magnetize in arbitrary direction. In continuous magnetization, neighboring sections cannot have sharp changes in magnetization, whereas discrete magnetization enable independent magnetization of adjacent sections. In reprogrammability, limited refers to reprogramming in directions designated during fabrication and technically challenging approaches at small scale. Actuated structure refers to the dimension of soft systems demonstrated in different approaches. In magnetic programming and fabrication, coupled refers to magnetic programming during the fabrication process and decoupled indicates magnetic programming afterwards the fabrication. In mass production, limited refers to restricted high-throughput production capability compared to lithography and roll to roll compatible methods.

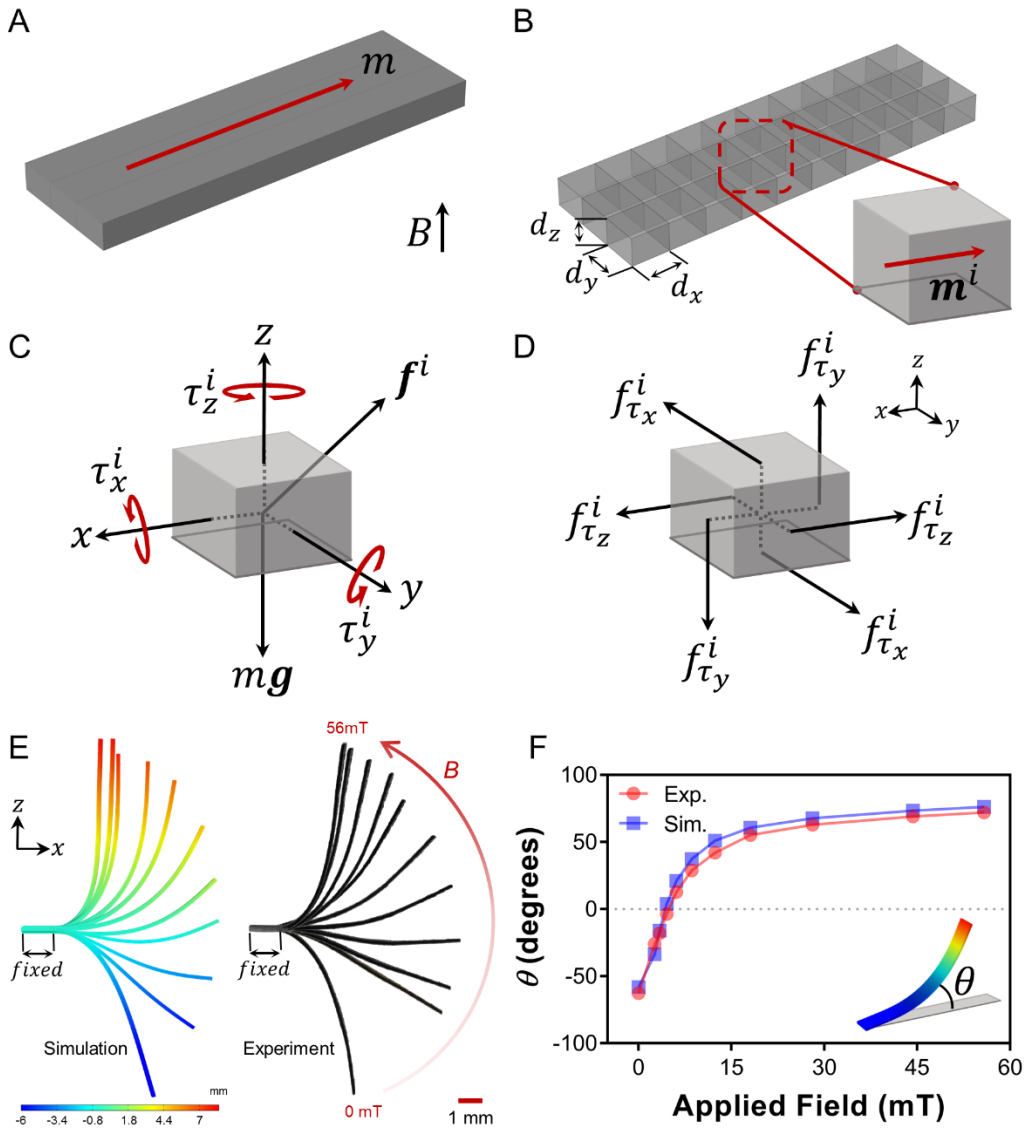

Figure S7. Computational modeling and validation of shape deformations. (A) A sample beam structure with a net magnetic moment $\boldsymbol{m}$. **(B)** The beam structures is divided into smaller sub-sections labeled by 'i' with the pre-defined lengths of d_x, d_y and d_z, and net magnetic moment $\boldsymbol{m}^i$. **(C)** Free body diagram of a subsection with $\boldsymbol{f}^i$, τ_x^i, τ_y^i, τ_z^i and $m\boldsymbol{g}$ representing magnetic force, magnetic torques on Cartesian axes, and gravitational force, respectively. **(D)** Distribution of the magnetic torques τ_x^i, τ_y^i, and τ_z^i as the boundary loads $f_{\tau_x}^i$, $f_{\tau_y}^i$, and $f_{\tau_z}^i$ on the subsection facets. **(E)** Simulation and experiment results for a beam (10 mm length x 1 mm width x 0.17 mm thickness) with a magnetization profile vertical to the applied external magnetic field. **(F)** Deflection angle (θ) values obtained from simulations and experiments depending on the applied external magnetic field.

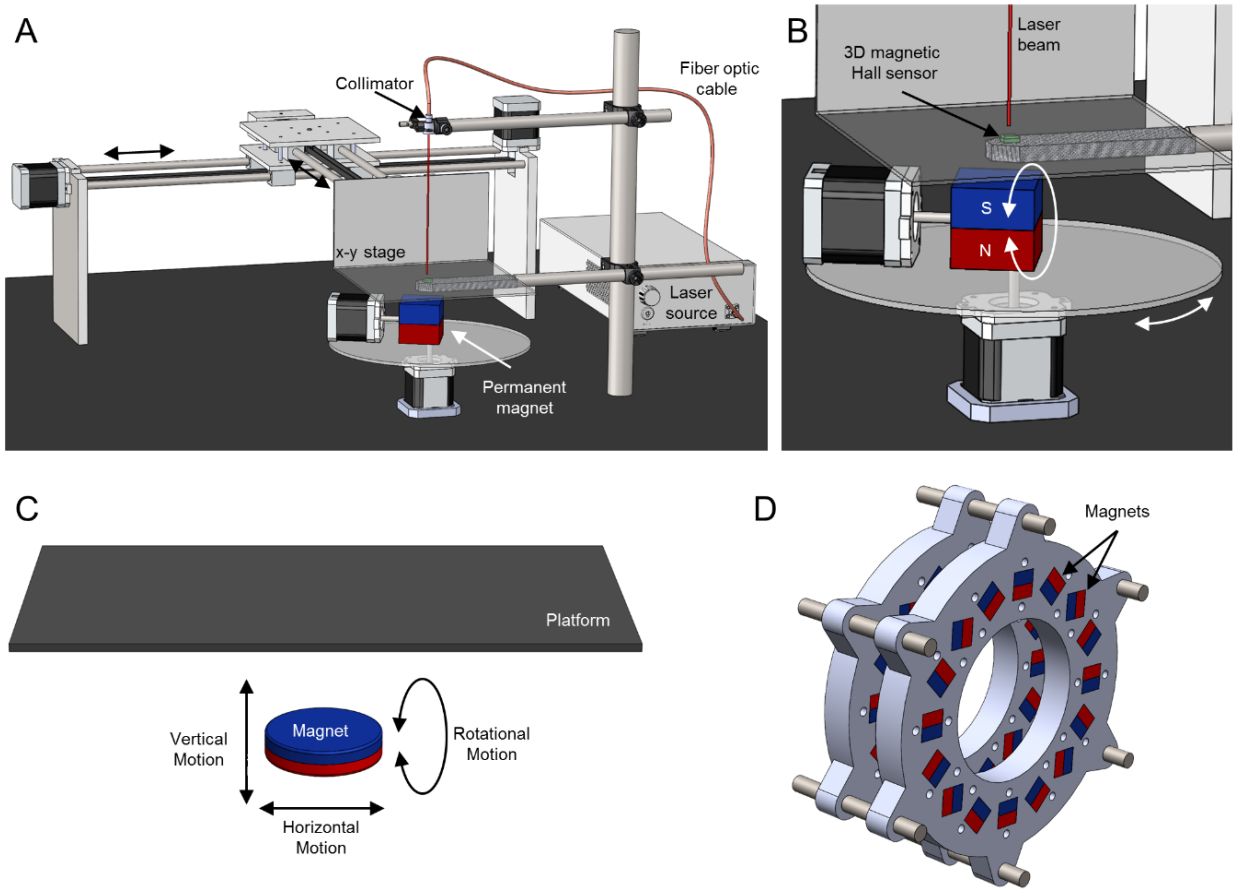

Figure S8. Heat-assisted magnetization and magnetic actuation setups. (A, B) Magnetization setup consists of a motorized stage, a NdFeB permanent magnet that can rotate in 360°, a 3D magnetic hall-effect sensor, and a power-adjustable fiber-coupled NIR laser with a collimator. **(C)** For magnetic actuation, a disc shaped magnet (60 mm diameter and 10 mm thick) was moved in vertical or horizontal directions, or rotated underneath an actuation platform. **(D)** A Halbach array, composed of 16 permanent magnets (10 mm x10 mm x 10 mm) arranged as shown, was used for generation of the uniform magnetic field for magnetic actuation.

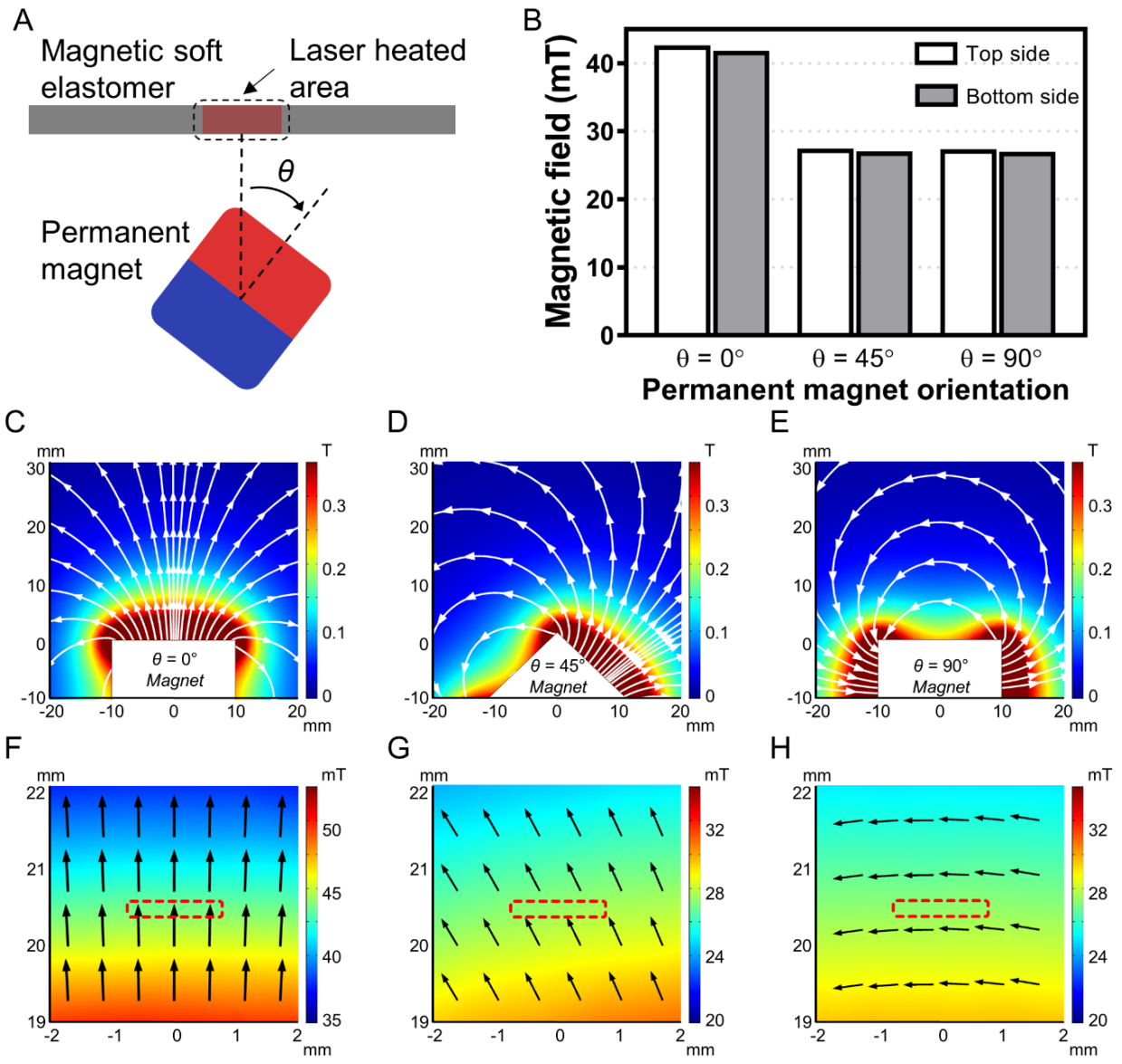

Figure S9. External magnetic field strength and uniformity in the laser-heated area for varying magnetization orientation. (A) Schematic of external permanent magnet and magnetic soft elastomer. **(B)** Magnetic field strength comparison at the magnetic soft elastomer bottom and top sides for permanent magnet orientations of 0°, 45°, and 90°. **(C-E)** Magnetic field strength and directions within the workspace of the permanent magnet at 0°, 45°, and 90° degrees, respectively. Color bar and white contours indicate the magnetic field strength and direction, respectively. **(F-H)** Enlarged plots of **(C)**, **(D)**, and **(E)** for a 3 mm x 4 mm area centered on the laser-heated sample location. Color bar, black arrows, and red dashed lines indicates the magnetic field strength, magnetic field direction, and the laser-heated area, respectively.

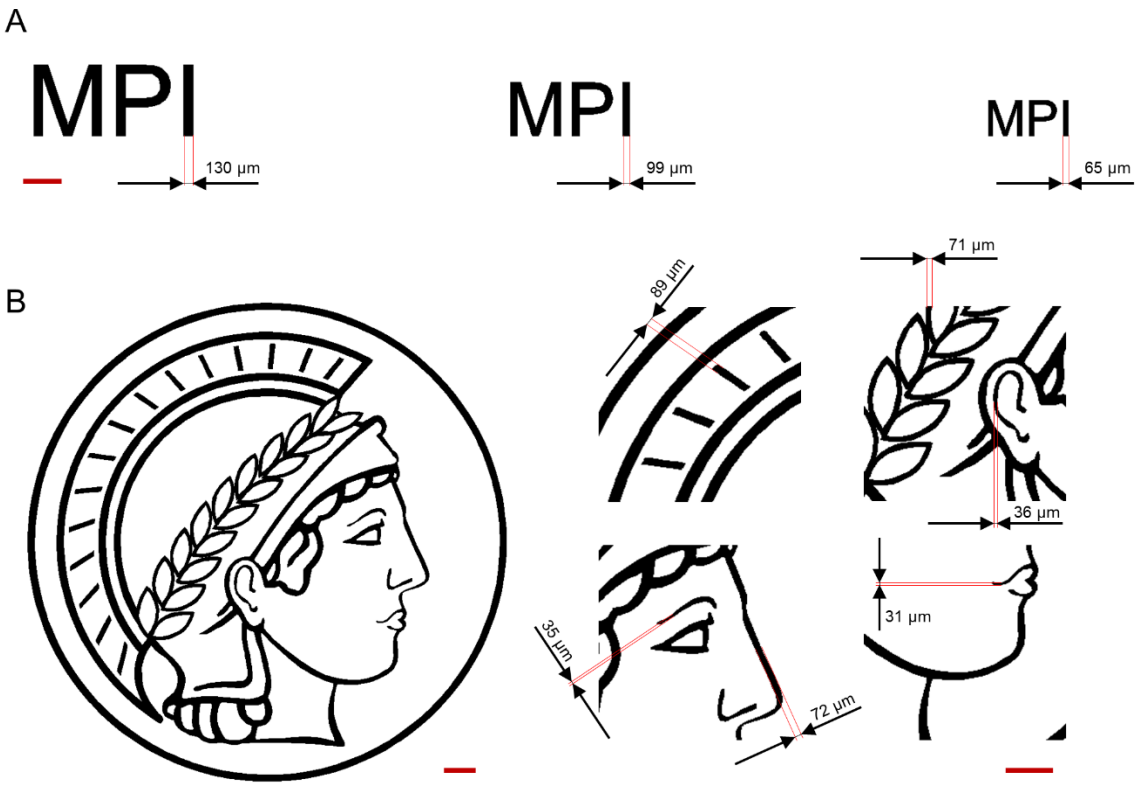

Figure S10. Photomask design. Critical dimensions employed in micropatterned laser heating **(A)** and fabrication of polyurethane NdFeB magnet for contact transfer of magnetic profiles **(B)**. Scale bars are 500 µm.

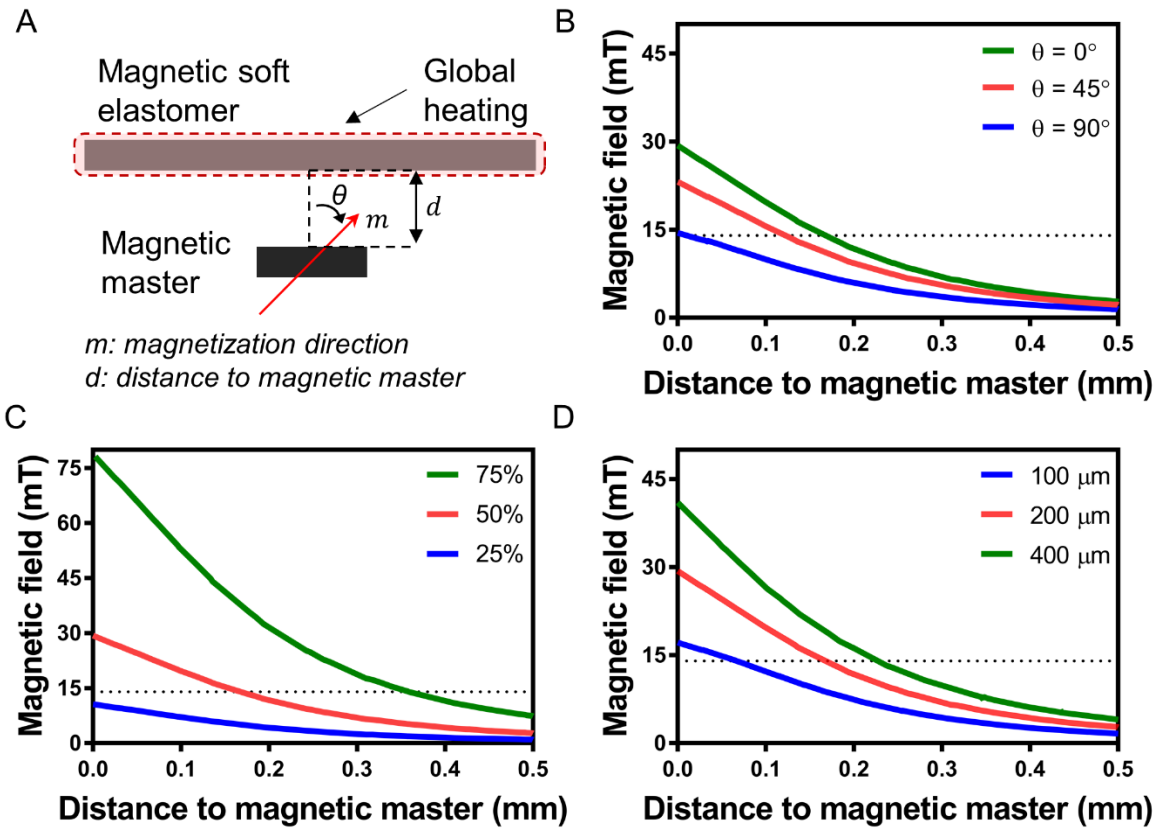

Figure S11. Magnetic field strength above the magnetic masters of varying magnetization directions, magnetic particle mass ratios, and thicknesses. (A) Schematic of magnetic master and magnetic soft elastomer. **(B)** Magnetic field strength for magnetic masters with magnetization directions of 0°, 45°, and 90°. **(C)** Magnetic field strength for magnetic masters with magnetic particle mass ratios of 75%, 50%, and 25%. **(D)** Magnetic field strength for magnetic masters with thicknesses of 100 μm, 200 μm, 400 μm. Dashed line at 14 mT shows the magnetization efficiency higher than 90%.

Supplementary Movies

Movie S1. 3D magnetically programmed flexible structures.

Movie S2. Reprogrammable magnetization of flexible and 3D structures.

Movie S3. Magnetically programmed micro petals.

Movie S4. Heat-assisted magnetic programming of soft materials.